# Directional Molecular Sliding at Room Temperature on a Silicon Runway†

**Xavier Bouju,*[a] Frédéric Chérioux,[b] Sébastien Coget,[b] Gwénaël Rapenne,[a,c] and Frank Palmino*[b]**

***Received Xth XXXXXXXXXX 20XX, Accepted Xth XXXXXXXXX 20XX***
***First published on the web Xth XXXXXXXXXX 200X***
**DOI: 10.1039/b000000x**

Design of working nanovehicules is a key challenge for the development of new devices. In this context, 1D controlled sliding of molecules on silicon-based surface is successfully achieved by using an optimized molecule-substrate pair. Even though molecule and surface are compatible, molecule-substrate interaction provides 1D template effect to guide molecular sliding along a preferential surface orientation. Molecular motion is monitored by STM experiments under ultra-high vacuum at room temperature. Molecule-surface interactions are elucidated by semi-empirical calculations.

## 1 Introduction

The fabrication of nanoscaled-machines[1] capable of providing work is one of the next challenges in the evolution of science at the nanometre scale. Technomimetic molecules[2] are daily life objects like gears, wheels, rotors or motors,[3–6] that have been miniaturized down to the molecular size. Molecular cars, which focus particular interest[7–10], have raised a very passionate research for fifteen years. This field of research was also boosted by the development of near-field microscopy such as Scanning Tunneling Microscopy (STM). Indeed, STM is known to be a powerful technique to observe the molecule/surface systems with sub-molecular resolution but also to monitor the molecular motion and to induce a displacement by tip/molecule interactions[11–15]. The design of molecular nanovehicules and the study of their single molecular motions are particulary interesting for the achievement of matter transport at the nanoscale. Since 2000, molecular motion proofs of concept have been achieved in the case of single molecules adsorbed onto noble metal surfaces under ultrahigh vacuum and at low temperature[7,8,10,16–18]. These surfaces have been chosen because their molecule-surface interactions are weak enough to provide molecular diffusion by thermal or light activation or by mechanical actuation with the STM tip. Nevertheless, directional controlled motion is still rare. For example, thermally activated motion often leads to Brownian (random) motion. Using 1D periodic surface or step edges leading to 1D template effect can induce transition from a 2D random motion to linear movement. Unfortunately, only few noble metal surfaces possess this type of nanostructuration (Cu-O/Cu[19], Au(111)[20] etc). By contrast, there are hundreds of metal-semiconductor interfaces with controlled periodicity and symmetry induced by metal adsorption onto semiconductors[21–24]. However, in the case of semiconductors, molecule-surface interactions are often too strong, which leads to a restricted molecular diffusion, even if using passivated surfaces can circumvent this drawback.[25–29] Here, we demonstrate that 1D SmSi reconstructions can be used as topographic and/or electronic nano-templates for guided molecular sliding along one surface orientation. Molecular diffusion has been monitored by STM at room temperature and the role of molecule-surface interactions has been elucidated by semi-empirical calculations.

## 2 Methods

### 2.1 Molecules

The 1,4-di-(9-ethynyltriptycene)benzene molecule (DETB) is built around a 1,4-diethynylbenzene axle with both sides equipped with a triptycene wheel[30–32]. This DETB molecule has been chosen because its length of 1.64 nm is close to the distance between two Sm rows of a SmSi interface (Fig. 1a).

### 2.2 Surface preparation and STM experiments

The SmSi interfaces were prepared by Sm evaporation from a Mo crucible onto clean Si(111)-(7×7) substrates held at 550 °C. The evaporation rate was close to 0.63 monolayer

† *Electronic Supplementary Information (ESI) available: Computational details, additional STM images and movies showing DETB molecules sliding on SmSi(111)-(7×1) reconstruction obtained from semi-empirical calculations. See DOI: 10.1039/b000000x.*

[a] *CEMES-CNRS, NanoSciences Group, 29 rue Jeanne Marvig, BP 94347, F-31055 Toulouse Cedex 4, France. Tel: +33 56225 7812; E-mail: xavier.bouju@cemes.fr*
[b] *Institut FEMTO-ST, Université de Franche-Comté, CNRS, ENSMM, 32, Avenue de l'Observatoire, F-25044 Besançon Cedex, France. Tel: +33 38199 4712; E-mail: frank.palmino@pu-pm.univ-fcomte.fr*
[c] *Université de Toulouse, UPS, CEMES, 29 rue Jeanne Marvig, BP 94347, F-31055 Toulouse Cedex 4, France*

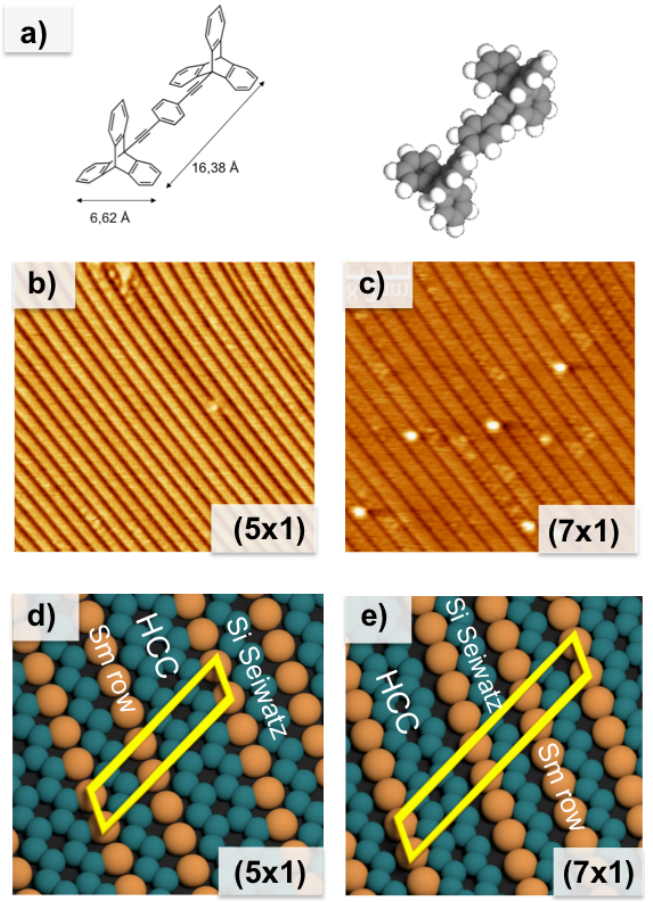


**Fig. 1** a) Chemical structure and CPK (Corey-Pauling-Koltun) model of the minimum energy conformation in gas phase of 1,4-di-(9-ethynyltriptycenyl)benzene molecule b) and c) STM images ($32\times32$ nm$^2$, $V_s = 2$ V, $I_t = 0.18$ nA) and d) and e) structural models of respectively, SmSi(111)-$5\times1$ and SmSi(111)-$7\times1$ reconstructions. Elementary cells are highlighted in yellow.

(ML) per minute. One ML of Sm is defined as one atom per $1\times1$ surface unit cell of the unreconstructed Si(111) surface (1 ML corresponds to $7.8\times10^{14}$ atoms per cm$^2$). The SmSi phase diagram exhibits, in the submonolayer range, three 1D reconstructions based on a combination of honeycomb chain channels (HCC), Seiwatz Si chains and rows of Sm atoms. These reconstructions appear on STM images as well-ordered row-like structures. Both ($5\times1$) and ($7\times1$) reconstructions are obtained respectively for 0.4 and 0.45 monolayer of Sm (Fig. 1b and 1c). The STM images appearance is characterized by large bright stripes. These stripes, attributed to Seiwatz Si chains and rows of Sm atoms, are separated by darker lines associated to the HCC structures[33–36]. The molecules were sublimed at 200 °C from a Kentax cell. STM Experiments were carried out in an ultrahigh vacuum chamber with a pressure lower than $1\times10^{-10}$ mbar equipped with an Omicron STM. Images were acquired at room temperature in the constant current mode. All STM images were analysed using WSxM software[37]. The artwork was produced with Blender[38].

## 3 Results and discussion

### 3.1 Deposition and motion of DETB on SmSi(111)-5×1 reconstruction

DETB molecules were initially adsorbed with a low molecular coverage (<0.2 monolayer) in order to determine their preferential adsorption site on SmSi(111)-$5\times1$ by STM experiments. On the basis of previous STM images obtained for DETB molecules deposited on other interfaces[16,23], the two paired protrusions observed in STM images (see Fig. 2a) are attributed to the two triptycene wheels of a single DETB molecule. Molecules are adsorbed onto large stripes between two dark rows (*i.e.* HCC). On the basis of DETB length (1.64 nm) and the distance between two HCC (1.66 nm), and on the basis of the structural model proposed for DETB adsorption on SmSi(111)-$8\times2$ surface[23], the DETB adsorption site on a SmSi(111)-$5\times1$ surface is depicted by the structural model shown on Fig. 2b. This adsorption site consists in two phenyl groups of each triptycene wheels adsorbed above two Sm chains. By increasing DETB coverage to 0.3 monolayer, most of the molecules appear self-aligned along the $[1\bar{1}0]$ direction forming short nano-lines (Fig. 2c), and a few single molecules remain. Moreover, few characteristic stripes corresponding to uncovered SmSi(111)-($5\times1$) are still observed. A number of fuzzy lines evidence molecule diffusion during the tip scanning (Fig. 2c). As the molecular motion is sufficiently slow, it is possible to record successive STM images to observe the trajectory of the molecule (see Fig. S1 in Supplementary Information). Such time-lapse images may evidence the molecular movement as already described.[39–41] However, this shifting or sliding does not occur along the entire STM scan direc-

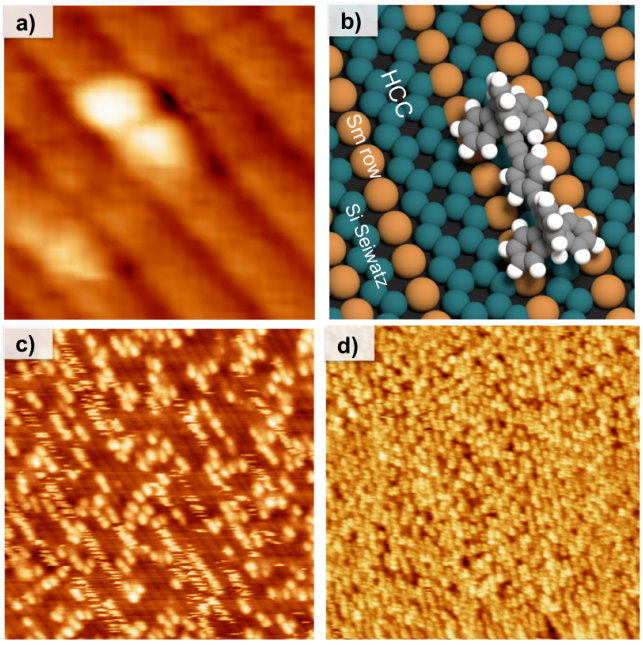


**Fig. 2** a) STM image of a single DETB molecule on SmSi(111)-5×1 reconstruction (7×7 nm$^2$, $V_s = 1.8$ V, $I_t = 0.7$ nA). b) DETB adsorption model on SmSi(111)-5×1 reconstruction. c) STM image for 0.3 monolayer molecule coverage (50×50 nm$^2$, $V_s = 2.6$ V, $I_t = 0.13$ nA). Frizzled stripes correspond to DETB diffusion along Sm rows. d) STM image for 0.9 monolayer molecule coverage showing DETB self-alignment (60×60 nm$^2$, $V_s = 2.2$ V, $I_t = 0.7$ nA).

tion (*i. e.* horizontal direction) but along the (5×1) stripes, between two HCCs. This noteworthy observation proves that this movement is guided by a strong 1D template effect of the surface. Due to the configuration of the DETB adsorption site on SmSi(111)-5×1, DETB slides with its main axis parallel to rows of Sm atoms. By increasing coverage rate up to the monolayer range, DETB nanolines aligned along Sm rows and covering all the substrate are observed on STM images (Fig. 2d), as previously observed on SmSi(111)-8×2 reconstruction[23]. At monolayer coverage, no DETB diffusion occurs due to steric hindrance. Subsequently, 1D molecular diffusion is achieved by using the template effect of the SmSi(111)-5×1 reconstruction thanks to the confinement of DETB molecules between two HCCs which act as two tracks. Nevertheless, DETB molecules retain their main axis parallel to the sliding direction, while DETB movements observed on copper surface occurred orthogonally to this axis[16]. Therefore, DETB adsorption and diffusion have been investigated on SmSi(111)-7×1 reconstruction, which possesses a wider spacing between HCC than SmSi(111)-5×1 reconstruction, respectively, 2.33 nm instead of 1.66 nm.

### 3.2 Deposition and motion of DETB on SmSi(111)-7×1 reconstruction

DETB molecules have been deposited at low molecular coverage (below 0.2 monolayer) in order to determine their adsorption sites on SmSi(111)-7×1 reconstruction by STM experiments at room temperature. As previously observed, DETB molecules appear as two bright protrusions in STM images (Fig. 3a). In contrast to SmSi(111)-8×2[23] and SmSi(111)-5×1 reconstructions, for which DETB molecules possess a single adsorption site corresponding to their principal axis being parallel to Samarium chains (*i. e.* along the $[1\bar{1}0]$ direction), on SmSi(111)-7×1 reconstruction, DETB molecules are here adsorbed on four different adsorption sites. Indeed, 86% of DETB molecules are adsorbed between two HCCs, showing three different orientations (noted 1,2 and 3 in Fig. 3), while around 14% of molecules are adsorbed above an HCC (orientation noted 4 in Fig. 3).

In the case of DETB molecules adsorbed between HCCs, the three different adsorption sites can be described with the help of high-resolution STM images. Orientation 1, involving 14% of molecules, consists in DETB molecules adsorbed with their main axis perpendicular to the Sm rows of the surface and with each of the two triptycene wheels above Sm rows (orientation 1, Fig. 3b). Orientation 2, which is the most commonly observed with 44% of molecules, corresponds to the adsorption site observed on 8×2 and 5×1 reconstructions[23], where DETB molecules are adsorbed parallel to Sm rows and with both triptycene wheels above Sm rows (orientation 2, Fig. 3b). Nevertheless, DETB molecules are not positioned on the centre line between two HCCs in the case of 7×1, unlike on 5×1 and 8×2, because on 7×1 reconstruction, there are three Sm rows between two HCCs instead of two Sm rows in 8×2 and in 5×1 reconstructions. Thus, DETB molecules seem prefer adsorption with triptycene blade above Sm rows. 28% of molecules are adsorbed in a third orientation with their main axis rotated by 20° from Sm rows and with two triptycene wheels above Sm rows (orientation 3, Fig. 3b). Finally and as already mentioned, 14% of molecules are adsorbed with one triptycene wheel above Sm rows while the other wheel is above an HCC (orientation 4, Fig. 3b).

At room temperature, DETB molecules are always motionless for orientations 3 and 4 whereas DETB diffusion is observed in the case of orientations 1 and 2. In the case of orientation 2, when the DETB main axis is parallel to Sm rows, DETB molecules slide spontaneously along these rows, as previously observed on 8×2 and on 5×1 reconstructions. In the case of orientation 1, when DETB molecules are perpendicular to Sm rows, molecular motion is highlighted by fuzzy STM lines (black arrow, (Fig. 4a)) which are assigned to molecule shifting during the STM scanning (Fig. 4b). At higher coverage ratio, DETB movement, with an axis orthogo-

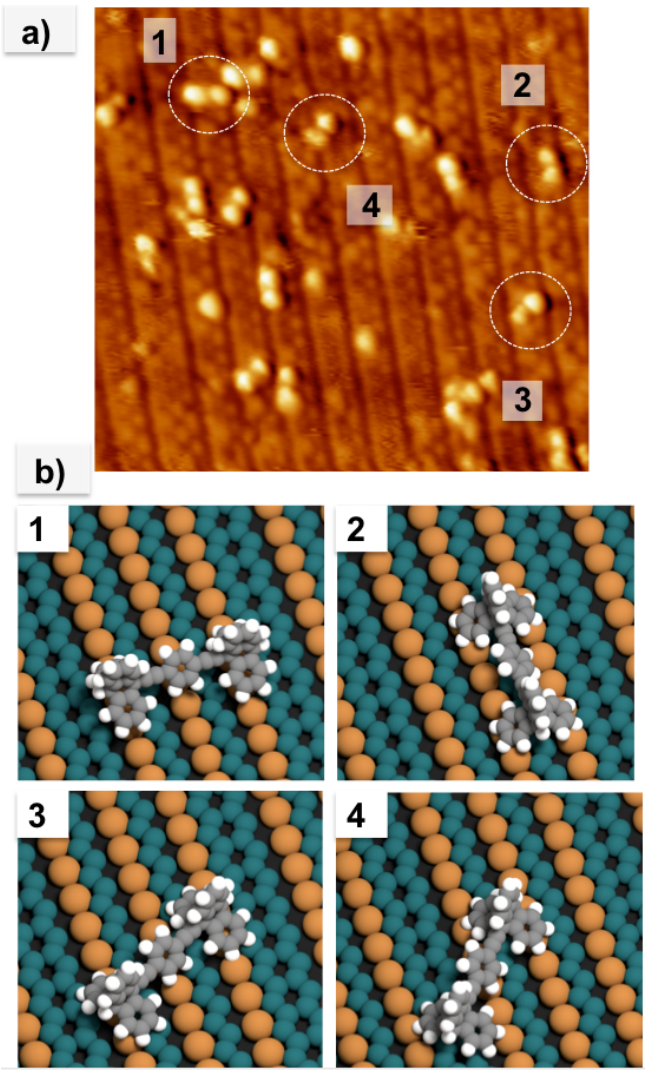


**Fig. 3** a) STM image (30×30 nm$^2$, $V_s = 2.0$ V, $I_t = 0.06$ nA) of DETB molecules on SmSi(111)-7×1 showing four different orientations highlighted with white dashed circles. b) Adsorption models corresponding to DETB orientations observed in STM image 3a)

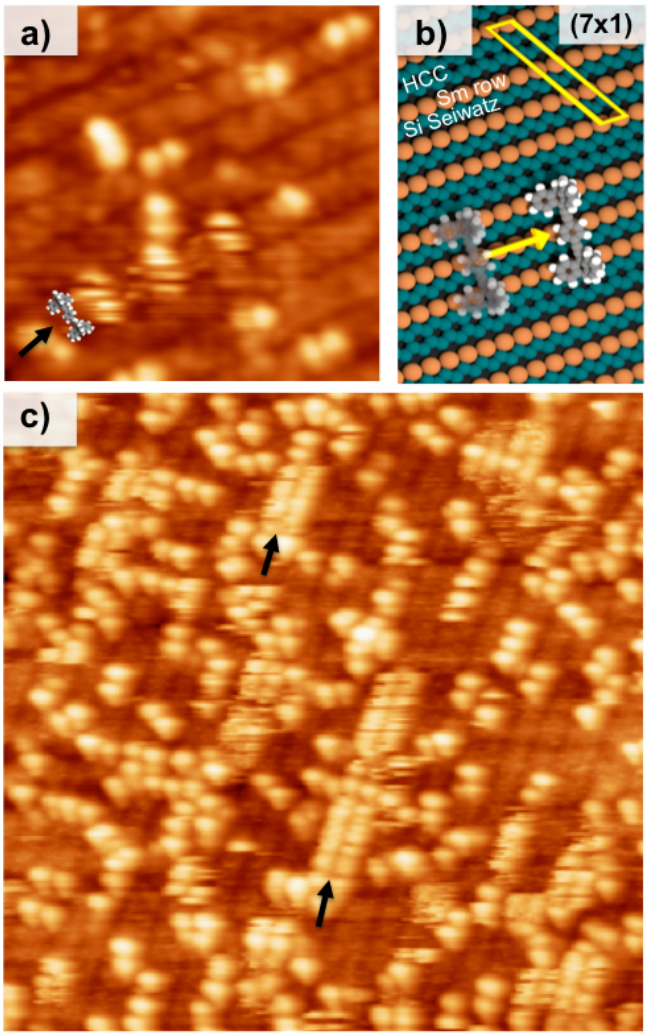


**Fig. 4** a) STM image of DETB molecules on SmSi(111)-7×1 at low DETB coverage (15×15 nm$^2$, $V_s = 1.8$ V, $I_t = 0.02$ nA). When DETB molecules are adsorbed with their main axis perpendicular to the surface $[1\bar{1}0]$ direction, a shifting along this direction is highlighted with a black arrow. b) Model of DETB sliding observed in 4a) Elementary cell is shown in yellow. c) STM image (40×40 nm$^2$, $V_s = 2.2$, $I_t = 0.1$ nA) recorded at higher DETB coverage, wherein four DETB orientations observed in Fig. 3a) are still observed. DETB sliding shown in 4a) leads to the formation of dual bands (black arrows).

nal to Sm rows, is observed by formation of dual frizzled band on STM images (Fig. 4c). In both cases, DETB molecules are sliding along Sm rows, despite the large distance between two HCCs (2.33 nm) compared to the DETB length (1.64 nm).

### 3.3 Semi-empirical calculations

The main objective of the calculations was to understand why the observed molecular motion is parallel to the Sm rows and why it remains confined between HCC chains while these channels are sufficiently far apart to allow some freedom in the movements. According to the recorded STM images, one expects mainly five typical motions of the molecule. To discuss these motions, we performed calculations to estimate the energy barrier the molecule has to overcome during each type of motion. These calculations have been tackled in a semi-empirical framework, based on the quantum chemistry approach of the atom superposition and electron delocalization molecular orbital (ASED-MO) theory.[42–44] An extension of this method is provided by the ASED+ code[45] which has proven its reliability with various molecular systems on metallic surfaces,[6,46,47] on insulating films,[48] or on semiconducting surfaces.[49,50] Computational details may be found in the Supplementary Information section. However, the purpose here is to estimate orders of magnitude rather than accurate values to qualitatively explain adsorbed motions. Five characteristic cases have been identified (Fig. 5) to discuss diffusion of the DETB molecule. Thus, by using ASED+ code, the DETB molecule is relaxed in 3D except a single hydrogen atom on the top of the molecule for which relaxation is allowed in the $z$ direction only. This atom serves as a marker to generate straight trajectories between successive adsorption sites. The first three cases (Fig. 5a-c) concern molecular sliding between two HCC domains with the DETB main axis parallel or perpendicular to Sm rows. In Fig. 5a, the sliding is parallel to Sm rows with the DETB main axis perpendicular to the Sm rows. The corresponding energy barrier is 0.35 eV, which is the smallest energy barrier calculated in this study. This value is in agreement with experimental STM observations where the diffusion with the process in Fig. 5a is mostly favoured as shown in Fig. 4a. Moreover, the DETB length fits well with the width of the channel formed by three Sm rows. We have also calculated the energy barrier to cross two consecutive channels (Fig. 5b) and we found an energy of 5 eV. This corresponds to a strong trapping in the Si Seiwatz/Sm rows and it is impossible for DETB molecules to escape out of Sm tracks at room temperature, as observed in STM experiments. This should explain as well the confinement above SM rows in the $5 \times 1$ reconstruction, generating molecular lines at high coverage (Fig. 2d). However, if confinement between HCCs is due to this strong energy barrier, DETB molecules may anyway rotate on themselves as the distance between HCCs is

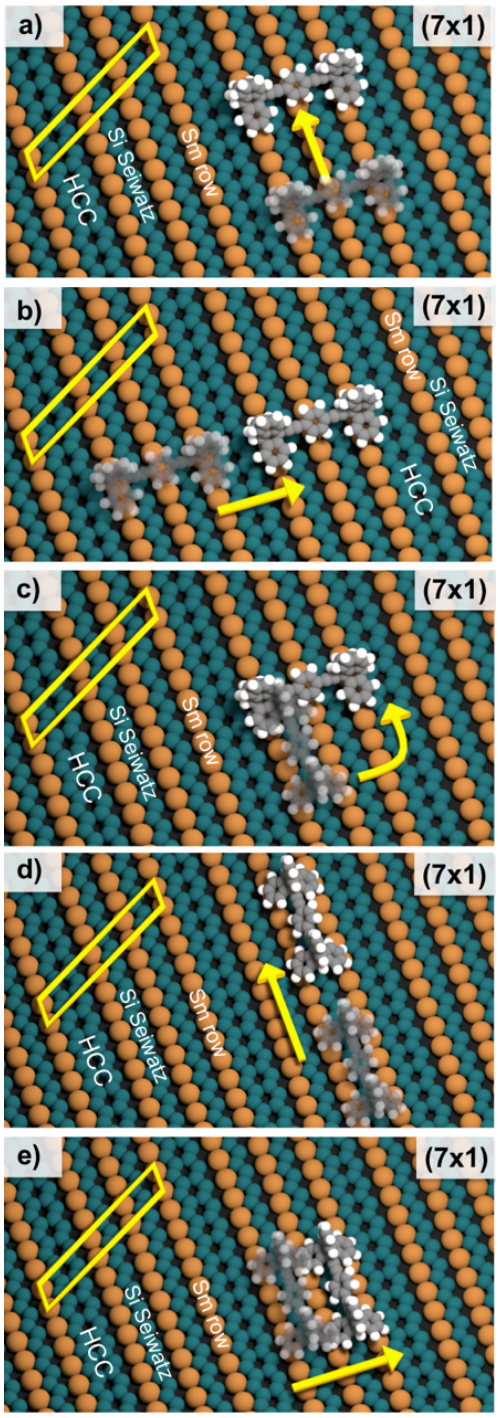


**Fig. 5** The five models simulated by ASED+ method, corresponding to possible DETB motions on SmSi(111)-7×1 reconstruction. Motions described in a) and d) have been experimentally observed by STM while motions described in b), c) and e) have not. Elementary cells are highlighted in yellow.

larger than the length of the DETB molecule (Fig. 5c). The energy barrier for this rotation is 0.5 eV, which is higher than the energy barrier corresponding to the sliding motion. Therefore, the propensity of the molecule to slide rather than to rotate between HCC channels on 7×1 reconstruction is observed with experimental STM data.

When the DETB main axis is parallel to an Sm row, (Fig. 5d-e), DETB molecules slide along Sm rows. This type of motion is observed on all the SmSi(111) reconstructions investigated. On 5×1 and 8×2 reconstructions, there are two Sm rows spaced by 0.664 nm. Therefore, the DETB molecules can only move parallel to Sm rows given the distance between two blades of the triptycene wheels (they are spaced by 0.662 nm, as estimated in the gas phase). In the case of the 7×1 reconstruction, there are now three Sm rows with the same interspacing, giving a 1.33 nm distance between rows 1 and 3, and the HCCs are separated by 2.33 nm. A DETB molecule could thus undergo two possible motions: sliding along Sm rows (Fig. 5d) or jumping from Sm rows 1 and 2 to Sm rows 2 and 3 (Fig. 5e). The energy barriers for sliding parallel to Sm rows (Fig. 5d) and for jumping between Sm rows (Fig. 5e) are 0.5 eV and 0.8 eV, respectively. This energy difference explains the reason why the sliding of DETB molecules remains confined on two Sm rows during STM experiments on 7×1 reconstruction. In addition, the energy barrier for DETB sliding along an Sm row is lower when the main axis of the molecule is perpendicular to the Sm rows (Fig. 5a, 0.35 eV), than when it is parallel (Fig. 5d, 0.5 eV). This difference explains why we observe experimentally preferential DETB sliding with its main axis perpendicular to Sm rows.

Finally, one would like to emphasize the key role of the central benzene ring of the molecule on the axle. Intuitively, it can be seen as a pawl combined to the the Sm row structure and constitutes a ratchet and pawl at the molecular level.[51–53] By following the conformational changes during the motion shown in Fig. 5a, the central ring is not always perpendicular to the surface plane, its successive orientations could explain the energy barrier height (see movies in Supplementary Information).

The deposition of molecules at room temperature leads to self-alignment along the Seiwatz rows, as already shown for the 8×2 reconstruction and as demonstrated in Fig. 2c and Fig. 4c. Thermal effects are thus responsible of the molecular diffusion. Moreover, tip-induced motions have been observed in particular cases but the probe during scanning is not systematically efficient to generate molecular motions.

## 4 Conclusion

In this study, we have demonstrated the essential role of molecule-surface interactions to control the movement of molecules on a semiconductor surface at room temperature. This dual mode of action of SmSi interfaces, acting as template both for static molecule deposition and for dynamic molecular motions. Joint surface engineering and molecular design enable us to put the field of atomic-scale matter transport on the tracks for the future development of promising nanodevices. With the ability to adjust the geometric parameters of the surface to those of the target molecule, it is now possible to promote its directional movement. This strategy should enable the development of nanodevices to transport matter or information at the molecular level on semiconductor surfaces.

## 5 Acknowledgements

This work was supported by Pays de Montbéliard Agglomération, the CNRS, the University Paul Sabatier of Toulouse and the French Agency ANR P3N (AUTOMOL project n°ANR-NANO-09-040). This work has been performed in cooperation with the Labex ACTION program (contract ANR-11-LABX-01-01). Part of this work was performed using High Performance Computing resources from the *CALcul en MIdi-Pyrénées* (CALMIP) facilities (Grant n°2011-[P0832]). XB thanks S. Monturet for fruitful discussions.

## References

1 V. Balzani, M. Venturi, A. Credi, Molecular Devices and Machine: Concepts and Perspectives for the Nanoworld. Wiley-VCH, Weinheim (2008).
2 G. Rapenne, Org. Biomol. Chem. **3**, 1165 (2005).
3 G. S. Kottas, L. I. Clarke, D. Horinek, J. Michl, Chem. Rev. **105**, 1281 (2005).
4 D. A. Leigh, F. Zerbetto, E. R. Kay, Angew. Chem. Int. Ed. **46**, 72 (2007).
5 N. Ruangsupapichat, M. M. Pollard, S. R. Harutyunyan, B. L. Feringa, Nature Chem. **3**, 53 (2011).
6 U. G. E. Perera, F. Ample, H. Kersell, Y. Zhang, G. Vives, J. Echevarria, M. Grisolia, G. Rapenne, C. Joachim, S.-W. Hla, Nature Nano. **8**, 46 (2013).
7 T. Kudernac, N. Ruangsupapichat, M. Parschau, B. Macia, N. Katsonis, S. R. Harutyunyan, K.-H. Ernst, B. L. Feringa, Nature **479**, 208 (2011).
8 C. Joachim, G. Rapenne, ACS Nano **7**, 11 (2013).
9 H. P. Jacquot de Rouville, R. Garbage, R. E. Cook, A. R. Pujol, A. M. Sirven, G. Rapenne, Chem. Eur. J. **18**, 46 (2012).

10 G. Vives, J. M. Tour, Acc. Chem. Res. **42**, 473 (2009).
11 F. Moresco, G. Meyer, K.-H. Rieder, H. Tang, A. Gourdon, C. Joachim, Phys. Rev. Lett. **86**, 672 (2001).
12 L. Bartels, G. Meyer, K.-H. Rieder, Phys. Rev. Lett. **79**, 697 (1997).
13 X. Bouju, C. Joachim, C. Girard, H. Tang, Phys. Rev. B **63**, 085415 (2001).
14 M. Yu, W. Xu, Y. Benjalal, R. Barattin, E. Lægsgaard, I. Stensgaard, M. Hliwa, X. Bouju, A. Gourdon, C. Joachim, T. R. Linderoth, F. Besenbacher, Nano Res. **2**, 254 (2009).
15 A. Nickel, R. Ohmann, J. Meyer, M. Grisolia, C. Joachim, F. Moresco, G. Cuniberti, ACS Nano **7**, 191 (2013).
16 L. Grill, K.-H. Rieder, F. Moresco, G. Rapenne, S. Stojkovic, X. Bouju, C. Joachim, Nature Nano. **2**, 95 (2007).
17 Y. Shirai, A. Osgood, Z. Yuming, K. F. Kelly, J. M. Tour, Nanolett. **5**, 2330 (2005).
18 G. Rapenne, J.-P. Launay, C. Joachim, J. Phys.: Condens. Matter **33**, S1797 (2006).
19 R. Otero, Y. Naitoh, F. Rosei, P. Jiang, P. Thostrup, A. Gourdon, E. Lægsgaard, I. Stensgaard, C. Joachim, F. Besenbacher, Angew. Chem. Int. Ed. **43**, 2091 (2004).
20 D. O. Bellisario, A. D. Jewell, H. L. Tierney, A. E. Baber, E. C. H. Sykes, J. Phys. Chem. C **114**, 14583 (2010).
21 M. H. Tuilier, C. Pirri, D. Berling, D. Bolmont, G. Gewinner, P. Wetzel, Surf. Sci. **555**, 94 (2004).
22 T. Roge, F. Palmino, C. Savall, J.-C. Labrune, C. Pirri, Surf. Sci. **383**, 350 (1997).
23 Y. Makoudi, E. Duverger, M. Arab, F. Chérioux, F. Ample, G. Rapenne, X. Bouju, F. Palmino, ChemPhysChem **9**, 1437 (2008).
24 F. P. Netzer, J. Phys. Condens. Matter **7**, 991 (1995).
25 B. Baris, J. Jeannoutot, V. Luzet, F. Palmino, A. Rochefort, F. Chérioux, ACS Nano **6**, 6905 (2012).
26 B. Baris, V. Luzet, E. Duverger, Ph. Sonnet, F. Palmino, F. Chérioux, Angew. Chem. Int. Ed. **50**, 4094 (2011).
27 Y. Makoudi, M. Arab, F. Palmino, E. Duverger, F. Chérioux, J. Am. Chem. Soc. **130**, 6670 (2008).
28 D. V. Gruznev, D. Chudenko, A. Zotov, A. Saranin, J. Phys. Chem. C **114**, 14489 (2010).
29 Y. Tanaka, P. Mishra, R. Tateishi, N. Thanh Cuong, H. Orita, M. Otani, T. Nakayama, T. Uchihashi, K. Sakamoto, ACS Nano **7**, 1317 (2013).
30 C. Joachim, H. Tang, F. Moresco, G. Rapenne, G. Meyer, Nanotechnology **13**, 330 (2002).
31 L. Grill, K.-H. Rieder, F. Moresco, G. Jimenez-Bueno, C. Wang, G. Rapenne, C. Joachim, Surf. Sci. **584**, 153 (2005).
32 G. Rapenne, G. Jimenez-Bueno, Tetrahedron **63**, 7018 (2007).
33 F. Palmino, E. Ehret, L. Mansour, J.-C. Labrune, G. Lee, H. Kim, J.-M. Themlin, Phys. Rev. B **67**, 195413 (2003).
34 E. Ehret, F. Palmino, L. Mansour, E. Duverger, J.-C. Labrune, Surf. Sci. **569**, 23 (2004).
35 F. Palmino, E. Ehret, L. Mansour, E. Duverger, J.-C. Labrune, Surf. Sci. **586**, 56 (2005).
36 F. Palmino, E. Duverger, Surf. Sci. **603**, 2771 (2009).
37 I. Horcas, R. Fernandez, J. M. Gomez-Rodriguez, J. Colchero, J. Gomez-Herrero, A. M. Baro, Rev. Sci. Instrum. **78**, 013705 (2007).
38 http://www.blender.org
39 Y. Shirai, A. J. Osgood, Y. Zhao, K. F. Kelly, J. M. Tour, Nano Lett. **5**, 2330 (2005).
40 Y. Shirai, A. J. Osgood, Y. Zhao, Y. Yao, L. Saudan, H. Yang, C. Yu-Hung, L. B. Alemany, T. Sasaki, J.-F. Morin, J. M. Guerrero, K. F. Kelly, J. M. Tour, J. Am. Chem. Soc. **128**, 4854 (2006).
41 P. L. E. Chu, L. Y. Wang, S. Khatua, A. B. Kolomeisky, S. Link, J. M. Tour, ACS Nano **7**, 35 (2013).
42 A. B. Anderson, Int. J. Quantum Chem. **49**, 581 (1994).
43 G. Calzaferri, L. Forss, I. Kamber, J. Phys. Chem. **93**, 5366 (1989).
44 M. Bosson, C. Richard, A. Plet, S. Grudinin, S. Redon, J. Comput. Chem. **33**, 779 (2012).
45 F. Ample, C. Joachim, Surf. Sci. **600**, 3243 (2006).
46 C. J. Villagomez, O. Guillermet, S. Goudeau, F. Ample, Hai Xu, C. Coudret, X. Bouju, T. Zambelli, S. Gauthier, J. Chem. Phys. **132**, 074705 (2010).
47 L. Vernisse, S. Munery, N. Ratel-Ramond, Y. Benjalal, O. Guillermet, X. Bouju, R. Coratger, J. Bonvoisin, J. Phys. Chem. C **116**, 13715 (2012).
48 Ch. Bombis, F. Ample, J. Mileke, M. Mannsberger, C. J. Villagómez, Ch. Roth, C. Joachim, L. Grill, Phys. Rev. Lett. **104**, 185502 (2010).
49 F. Ample, C. Joachim, Surf. Sci. **602**, 1563 (2008).
50 A. Bellec, F. Ample, D. Riedel, G. Dujardin, C. Joachim, Nano Lett. **9**, 144 (2009).
51 R. D. Astumian, Science **276**, 917 (1997).
52 F. Chiaravalloti, L. Gross, K.-H. Rieder, S. M. Stojkovic, A. Gourdon, C. Joachim, F. Moresco, Nature Mat. **6**, 30 (2006).
53 K.-H. Ernst, Nature Nano. **8**, 7 (2013).